Environmental Science: Atmospheres

ROYAL SOCIETY OF CHEMISTRY

PAPER

View Article Online
View Journal

Check for updates

Cite this: DOI: 10.1039/d5ea00139k

The effect of surface sink saturation and emission altitude on hydrogen's atmospheric impact

Evan M. Gibney, [a] Sebastian D. Eastham, [b] Florian Allroggen[a] and Raymond L. Speth *[a]

Hydrogen is often viewed as a potential component of a decarbonized transportation system, offering the ability to eliminate direct CO_2 emissions while being produced with low lifecycle greenhouse gas emissions. However, direct emissions of hydrogen can trigger indirect climate and air quality effects which may partially or fully offset these benefits. We use the GEOS-Chem High Performance (GCHP) global chemistry-transport model to investigate how surface sink representation and emission altitude influence the climate impact of hydrogen emissions, specifically with respect to high-altitude emissions from prospective future hydrogen aircraft. We show that if the soil sink becomes saturated and can no longer increase uptake rates as atmospheric hydrogen concentrations rise, the perturbation lifetime of hydrogen increases, leading to a 3.8-fold increase in hydrogen's climate impact over 100 years compared to an unsaturated sink. We demonstrate that if the soil sink is unsaturated, hydrogen emitted at commercial aircraft cruise altitudes (~11 km) has a greater climate impact than equivalent surface emissions. The magnitude of this additional impact varies between 8% over a 20-year horizon to 13% over 100 years. This altitude sensitivity results from the vertical separation between high-altitude hydrogen emissions and the soil sink, which increases the likelihood of removal by OH. Our findings highlight the need to prioritize mitigation of high-altitude hydrogen emissions, such as those from potential future hydrogen-fueled aircraft, compared to surface hydrogen emissions. More broadly, they reveal the limitations of fixed-boundary condition models to capture these mechanisms, underscoring the importance of transitioning to surface sink representations that can capture dynamic soil uptake responses. Constraining the real-world behavior of the soil sink remains a key research priority for accurately assessing hydrogen's climate impacts.

Received 22nd October 2025
Accepted 27th February 2026

DOI: 10.1039/d5ea00139k

rsc.li/esatmospheres

Open Access Article. Published on 09 March 2026. Downloaded on 4/20/2026 5:36:04 AM.
This article is licensed under a Creative Commons Attribution 3.0 Unported Licence.

Environmental significance

Hydrogen's potential to negatively affect atmospheric chemistry and climate through direct emissions remains uncertain, but could become important given the anticipated growth in hydrogen production, distribution, and use in a future hydrogen economy. This study examines two factors shaping hydrogen's climate impact: (1) emission altitude, and (2) the capacity of soil bacteria to absorb additional hydrogen when exposed to increasing hydrogen concentrations. We find that in the event that the hydrogen sink becomes saturated, whether from environmental changes such as rising temperatures, habitat loss from climate change and human activity, or from non-linearities in microbial uptake, the overall climate impact of hydrogen emissions is increased by a factor of 3.8 compared to conditions where the sink is not saturated. We also find that upper-tropospheric hydrogen emissions have 13% greater warming impact than equivalent emissions from the surface. These findings highlight the need for more accurate representations of soil uptake in atmospheric models and emphasize that the climate benefits of a hydrogen economy will depend not only on how much hydrogen is emitted, but also where and under what environmental conditions those emissions occur.

1 Introduction

Hydrogen produced with low lifecycle emissions offers a promising pathway to reduce climate and air quality impacts from fossil fuel use across multiple sectors.[1] However, these benefits may be partially offset by indirect warming impacts resulting from fugitive emissions of hydrogen which occur during production, transportation, distribution, and end-use.[2–5] Once released into the atmosphere, hydrogen can be removed by one of two pathways: (1) uptake by the microbial soil sink, which accounts for approximately 70–80% of the current hydrogen sink, or (2) oxidation by the hydroxyl radical (OH), which accounts for the remainder.[6–9] In the first case, hydrogen is metabolized by soil bacteria and removed from the atmosphere without otherwise perturbing the atmospheric composition.

[a]Laboratory for Aviation and the Environment, Department of Aeronautics and Astronautics, Massachusetts Institute of Technology, Cambridge, MA, USA. E-mail: speth@mit.edu

[b]Brahmal Vasudevan Institute for Sustainable Aviation, Department of Aeronautics, Imperial College London, London, UK

© 2026 The Author(s). Published by the Royal Society of Chemistry

Open Access Article. Published on 09 March 2026. Downloaded on 4/20/2026 5:36:04 AM. This article is licensed under a Creative Commons Attribution 3.0 Unported Licence.

However, in the second case, oxidation of hydrogen introduces competition with methane and non-methane volatile organic compounds (NMVOCs) for available OH. This in turn leads to an increased lifetime of methane, increased tropospheric ozone production, and increased burden of stratospheric water vapor, all of which are greenhouse gases contributing to warming.[3,4,10]

Extending the atmospheric lifetime of methane and delaying its eventual oxidation not only enhances its integrated warming impact, but also alters the timing and spatial distribution of its oxidation products, including ozone and water vapor. This is because while an individual methane molecule may remain in the atmosphere for longer it is still likely to be oxidized by OH, but at a later time. Assuming constant background conditions, the total amount of ozone produced by the methane then remains the same. This raises an important question: to what extent does the fate of an emitted molecule of hydrogen depend on the timing and location of its emission? The answer likely depends on the future behavior of the soil sink, which may evolve in response to rising temperatures, habitat loss from climate change and human activity, and non-linearities in microbial uptake.[8] Historical observations of increasing atmospheric hydrogen concentrations suggest that the soil sink is both insufficient to fully offset anthropogenic emissions and is variable over time.[9] Understanding how these limitations and potential future changes affect hydrogen's atmospheric impacts is therefore essential for accurately evaluating the climate impact of hydrogen.

In the context of aviation, improving our understanding of these processes is important as the industry is advancing the development of hydrogen-fueled aircraft in an effort to reduce its environmental impacts. Unlike other sectors, aviation could emit hydrogen at cruise altitudes in the upper troposphere and lower stratosphere, where the chemical and transport dynamics differ from the surface. To date, the impact of hydrogen emissions at altitudes where aircraft operate is not well understood. Due to the vertical mixing timescale of the troposphere, hydrogen emitted at altitude may have an increased average time before reaching the surface where it can interact with the soil sink. As a result, it may be more likely to be removed by oxidation with OH, potentially bypassing the soil sink due to the vertical separation of the loss pathways. While it typically takes about one week for air masses to become vertically mixed throughout the troposphere[11] and the lifetime of hydrogen against loss to OH is approximately 8 years,[12,13] changes in the initial conditions of hydrogen's emissions may bias how these two time scales interact with respect to hydrogen's removal. Capturing this behavior requires a better understanding of how soil uptake responds under changing environmental conditions and an accurate representation of hydrogen's transport dynamics.

Estimates of the current sink strength range from 55 to 88 Tg per year.[8] Uptake is regulated by high-affinity hydrogen-oxidizing bacteria (HA-HOB), microbes found in soil which are capable of metabolizing hydrogen at low concentrations present in the atmosphere. The efficiency of uptake is influenced by abiotic factors such as soil temperature and moisture, which govern diffusive transport, as well as biotic factors like the metabolic activity of HA-HOB. The metabolic activity of HA-HOB depends on atmospheric hydrogen concentrations, with hydrogen uptake rates increasing non-linearly as hydrogen availability rises.[8,14,15] Thus, future deposition rates of hydrogen may be enhanced by an increased atmospheric burden of hydrogen, potentially buffering the overall atmospheric impact of future hydrogen emissions. Conversely, any future saturation of the soil sink could amplify the climate impact of hydrogen emissions. Laboratory studies, while limited in number, suggest that even under the most extreme projections of future hydrogen use, global atmospheric hydrogen concentrations are likely to remain below saturation thresholds.[8] Specifically, experiments by Piché-Choquette *et al.* and Greening *et al.* show that saturation mechanisms only become dominant at hydrogen concentrations 50 to 100 times above current atmospheric levels.[14,16] Nevertheless, uncertainty remains regarding the response of microbial hydrogen uptake to changing environmental conditions. While complete global saturation is unlikely, localized or partial saturation could occur due to land-use change, soil degradation, or climate-driven shifts in microbial activity.

The indirect warming effects of hydrogen have gained research attention over the past decades. Early studies quantified the tropospheric methane and ozone response to surface hydrogen emissions using both simplified atmospheric chemistry models and higher fidelity 3-D models. For example, Derwent *et al.* first used a global box model, then later used a chemistry-transport model to calculate a global warming potential (GWP) for hydrogen of 5 ± 1 on a 100-year time horizon.[5,17] More recent studies have also quantified stratospheric water vapor impacts which were previously neglected.[8,10,18,19] Paulot *et al.* used the GFDL-AM4.1 Earth System Model to quantify this effect and found that it accounted for approximately a third of hydrogen's overall climate impact.[8] Warwick *et al.* calculated a GWP-100 of 12 ± 5 for hydrogen, with several other analyses finding values within this range.[10,13,18–21] Sand *et al.* also calculated a GWP-100 for hydrogen of 11.6 ± 2.8 through a multi-model assessment.[22] Recent work by Yang *et al.*, however, shows that the GWPs from these latest studies may be overestimated by up to 20% due to model biases in OH concentration and reactivity.[23]

Together, these studies have deepened our understanding of hydrogen's role in atmospheric chemistry and climate change, providing more refined estimates of its global warming potential and key sensitivities. It is now important to examine the uncertainties that remain, particularly the role of the soil sink in modulating hydrogen's impacts. Many studies, for instance, have modeled the soil sink using fixed surface boundary conditions, which hold the surface concentration of hydrogen at a preset value. This approach has been useful for capturing the general atmospheric response to hydrogen emissions, but may obscure feedback processes between hydrogen, methane, and ozone. This is because when the surface concentration of hydrogen is fixed, emitted hydrogen cannot properly persist and may be immediately removed at the surface prior to reacting with OH, effectively increasing the rate of surface uptake.

The limitations of fixed boundary conditions for methane have previously been studied in the context of aviation NO_x

 © 2026 The Author(s). Published by the Royal Society of Chemistry

Open Access Article. Published on 09 March 2026. Downloaded on 4/20/2026 5:36:04 AM. This article is licensed under a Creative Commons Attribution 3.0 Unported Licence.

emissions, where NO_x-induced ozone production leads to long-term methane reductions that partially offset the initial short-term warming response.[24] Khodayari *et al.* demonstrated that this long-term methane reduction can be approximated using feedback factors to capture the change in methane burden and lifetime.[25] However, this approach fails to capture the secondary effects of methane on the distribution of coupled species such as ozone and water vapor, which is also applicable to the atmospheric response to hydrogen emissions.[26,27] Moreover, previous studies have shown that the methane feedback factor varies between models. Recent analyses of hydrogen's atmospheric impacts report methane feedback factors ranging from 1.3 to 1.6, contributing to differences in the methane-related component of hydrogen's climate effect.[20,22] Incorporating more flexible representations of the soil sink through calibrated fluxes or physical deposition-based representations can help capture these coupled responses, which may be obscured under the fixed boundary condition and feedback factor framework.

Several previous studies on hydrogen have implemented various deposition-based schemes to model surface uptake based on historical observations of the surface sink and environmental factors such as soil temperature and moisture level. However, these models do not capture the potential for adaptation or saturation of the soil sink in response to rising atmospheric hydrogen concentrations, primarily due to a lack of data to quantify this process.[8,28] While there is still uncertainty surrounding this behavior, the potential implications of excluding this response warrant further investigation, as models independent of atmospheric hydrogen levels may misrepresent hydrogen's atmospheric lifetime and associated climate impacts.

In this study, we use calibrated flux boundary conditions for both hydrogen and methane to provide the first assessment of how the altitude of hydrogen emissions influences its atmospheric impact and how this process depends on surface uptake assumptions which adapt to atmospheric hydrogen concentrations. To assess the sensitivity of the climate response to soil uptake behavior, we simulate both saturated and unsaturated sink conditions, providing a range of possible outcomes under different sink assumptions. For each scenario, we conduct a 36-year atmospheric chemistry simulation with annually recurring emissions, including radiative transfer calculations to quantify the resulting climate impacts.

2 Methods

We simulate the atmospheric impacts of hydrogen when emitted from either the surface or the upper troposphere at an altitude of approximately 11 km, representative of a typical cruise altitude for commercial subsonic aircraft. For each of the two emission altitudes, we perform two simulations that vary the representation of the soil sink to model a range of uptake conditions and saturation behavior. The soil sink models are described in the surface boundary conditions section, and are presented in Table 1. Each of the four scenarios considers 1 Tg of hydrogen emitted uniformly (constant kg m^{-3} s^{-1}) on an annual, recurring basis, between 30° N and 60° N. This specific latitude range was selected to be representative of the overall aviation fuel burn distribution, where approximately 60% occurs within the 30° N and 60° N band, and approximately 90% occurs in the Northern Hemisphere.[29] Localizing the emissions in this way allows for clear observation of the resulting transport and chemical response, including inter-hemispheric exchange, which may appear spatially diffuse and difficult to isolate if emissions were distributed according to the exact aviation fuel burn pattern. In addition to the four scenarios described below, we perform a fifth simulation to use as a reference in which no additional hydrogen is emitted. Finally, we perform additional sensitivity simulations which test the effect of the background atmosphere on hydrogen's atmospheric impact, and consider an idealized upper bound scenario for hydrogen soil uptake. Together, these scenarios encompass a controlled range of plausible and extreme soil uptake behaviors, allowing us to assess the climate impact of hydrogen emissions across each scenario.

2.1 Global atmospheric modeling

We use the global chemistry-transport model GEOS-Chem 14.2.3 as implemented in GEOS-Chem High Performance (GCHP)[30] to evaluate the global chemistry and transport of atmospheric species in response to the hydrogen perturbations described in Table 1. The horizontal grid is represented as a cubed-sphere and all simulations are run with 24 horizontal divisions per cube edge (C24 resolution). This corresponds to an average grid spacing of 380 km. All simulations are run with 72 vertical layers, starting at the surface and ending at a pressure of 1 Pa. The vertical grid is parameterized by a hybrid-sigma representation.

Meteorological conditions are prescribed using data from the NASA Global Modeling and Assimilation Office's Modern Era Retrospective analysis for Research and Applications v2 (MERRA-2).[31] All simulations are integrated in time for a total of 36 years using four iterations of meteorological data from July 2010 to July 2019. Since the fate of emissions in the atmosphere is sensitive to background conditions, it is important to model a representative atmosphere for a hydrogen economy. Here, we select the Shared Socioeconomic Pathway (SSP) and radiative forcing scenario SSP1-2.6 as defined in the IPCC's sixth assessment report,[1] with a background atmosphere based on projected 2050 conditions. This pathway is chosen on the assumption that in a future where hydrogen achieves large scale market penetration, it is likely that other industries significantly

Table 1 Overview of hydrogen emission scenarios simulated

Scenario name	Location of H_2 emissions	H_2 soil sink model
Sur_Sat	Surface	Saturated
Alt_Sat	Altitude (~11 km)	Saturated
Sur_MM	Surface	Unsaturated, Michaelis–Menten
Alt_MM	Altitude (~11 km)	Unsaturated, Michaelis–Menten

Open Access Article. Published on 09 March 2026. Downloaded on 4/20/2026 5:36:04 AM. This article is licensed under a Creative Commons Attribution 3.0 Unported Licence.

reduce their greenhouse gas emissions. This rationale is particularly applicable for difficult-to-abate sectors like aviation, in which the presence of a large fleet of hydrogen aircraft may only be realistic in a future economy where other sectors have already successfully decarbonized. Independent of this socio-economic context, however, we also perform an additional reduced-length sensitivity simulation using the SSP2-4.5 scenario to assess the robustness of our conclusions to an alternative background atmosphere. Data from the Coupled Model Inter Comparison Project Phase 6 (CMIP6)[32] is used to represent the 2050 SSP1-2.6 and SSP2-4.5 atmospheres and emissions. Prior to the start of the 36-year simulations, we perform scaling of long-lived species in the default GEOS-Chem initialization (restart) file, followed by a 9-year spin-up simulation.

2.2 Surface boundary conditions

We replace the default GCHP fixed surface boundary conditions for both methane and hydrogen with saturated and unsaturated flux boundary conditions. In this context, "saturation" refers to a scenario in which the soil sink is unable to remove hydrogen at rates beyond present day levels. This representation provides a lower bound on hydrogen soil uptake and helps quantify the maximum climate impact of hydrogen emissions. Alternatively, the unsaturated sink is assumed to increase in strength as atmospheric hydrogen levels rise. While saturated flux boundary conditions have been previously applied to methane,[27] our study represents the first implementation for hydrogen within GEOS-Chem. Although fixed boundary conditions with feedback factors have previously been shown to produce accurate predictions of changes to methane lifetimes and burdens,[25] they can fail to capture long-term feedbacks in ozone production and other linked chemical species.[26] For studies on hydrogen's climate impacts, this is particularly important due to the coupling of the H_2–CH_4–CO–O_3 chemical system.[13]

To implement the saturated flux boundary condition, we begin with a 36-year calibration simulation using fixed surface boundary conditions for both hydrogen and methane. During this simulation, we archive the net monthly mean surface fluxes of hydrogen and methane at each grid cell required to maintain the prescribed surface mixing ratios. These archived values represent the combined effects of all emission and removal processes at the surface and quantify the net exchange with the atmosphere (*i.e.*, emissions minus losses). In subsequent simulations, we disable the fixed surface boundary condition and prescribe the monthly mean archived net fluxes as surface emissions. A sample of these calculated fluxes for hydrogen and methane is shown in Fig. 1. We find that our calculated fluxes, averaging −16.8 Tg H_2 per year and +561 Tg CH_4 per year, are consistent with the reported uncertainty ranges in the literature. For example, Paulot *et al.* report a global emission rate of 32.3 [29.9 to 37] Tg H_2 per year and a dry deposition sink of 54.7 [53.5 to 56.3] Tg H_2 per year, corresponding to a net surface exchange of −22.4 [−26.4 to −16.5] Tg H_2 per year.[8] Similarly, the global hydrogen budget by Ouyang *et al.* provides a central estimate of the net surface exchange of hydrogen of −18.5 Tg per year.[33] For methane, Saunois *et al.* provide an estimate of +538 [505 to 567] Tg CH_4 per year in net emissions at the surface.[34] We also calculate the hydrogen chemical production from photolysis of formaldehyde in GCHP to be 40.8 Tg H_2 per year, consistent with previous estimates.[8,33] Solving the hydrogen mass balance equation at steady-state, we calculate a baseline loss partitioning of 67.6% to soil uptake and 32.4% *via* oxidation by OH, which is also in line with the partitioning estimates from past studies.

Building on the standard, saturated flux boundary condition, we also introduce a new unsaturated flux boundary condition for hydrogen to represent a dynamic soil sink that actively responds to elevated atmospheric hydrogen concentrations. This formulation represents a physically motivated and realistic representation of microbial soil uptake under unsaturated conditions. Given the current limitations in the physical understanding of the hydrogen soil sink mechanism, we present this model not to precisely predict uptake rates, but to demonstrate how varying assumptions about the soil sink could affect hydrogen removal and the overall climate impact of hydrogen emissions. Here, we assume diffusive limitations are implicitly represented in the flux calibration process, and focus our model on capturing biotic responses to hydrogen exposure.

The dynamic approach uses a Michaelis–Menten kinetic model[35] to describe changes in hydrogen uptake by soil as a function of hydrogen exposure. The general form is $d[H_2]/dt = V_{max}[H_2]/(k_m + [H_2])$, where the uptake rate, $d[H_2]/dt$, depends on the surface concentration of hydrogen, $[H_2]$, and is governed by two parameters: the half-saturation constant, k_m, and the maximum rate of uptake, V_{max}.

$$\frac{d[H_2]}{dt} = \frac{[H_2]}{k_m + [H_2]} V_{max} \quad (1)$$

We set k_m to a value of 40 ppmv based on Piché-Choquette *et al.*'s experiments characterizing HA-HOB under varying hydrogen exposure levels.[14] Physically, this parameter represents the exposure level at which hydrogen reaches half of its maximum uptake rate in soil. As this threshold is several orders of magnitude above the most extreme future projections for atmospheric hydrogen concentrations,[16] global uptake rates are likely to remain far from saturation, and the model effectively reduces to a near-linear response at current atmospheric hydrogen levels.

To integrate this model into GCHP, we rearrange eqn (1) to derive a monthly scale factor, λ, which adjusts the calibrated hydrogen fluxes according to the change in the simulated surface concentration of hydrogen, $[H_2]_{sim}$, relative to the reference case, $[H_2]_{ref}$.

$$\lambda = \frac{[H_2]_{sim}}{[H_2]_{ref}} \left(\frac{k_m + [H_2]_{ref}}{k_m + [H_2]_{sim}} \right) \quad (2)$$

We then apply this scale factor to generate dynamically-updated monthly fluxes, F_{new}. Since GCHP does not explicitly prescribe hydrogen emissions, we assume a constant global

© 2026 The Author(s). Published by the Royal Society of Chemistry

Open Access Article. Published on 09 March 2026. Downloaded on 4/20/2026 5:36:04 AM.
This article is licensed under a Creative Commons Attribution 3.0 Unported Licence.

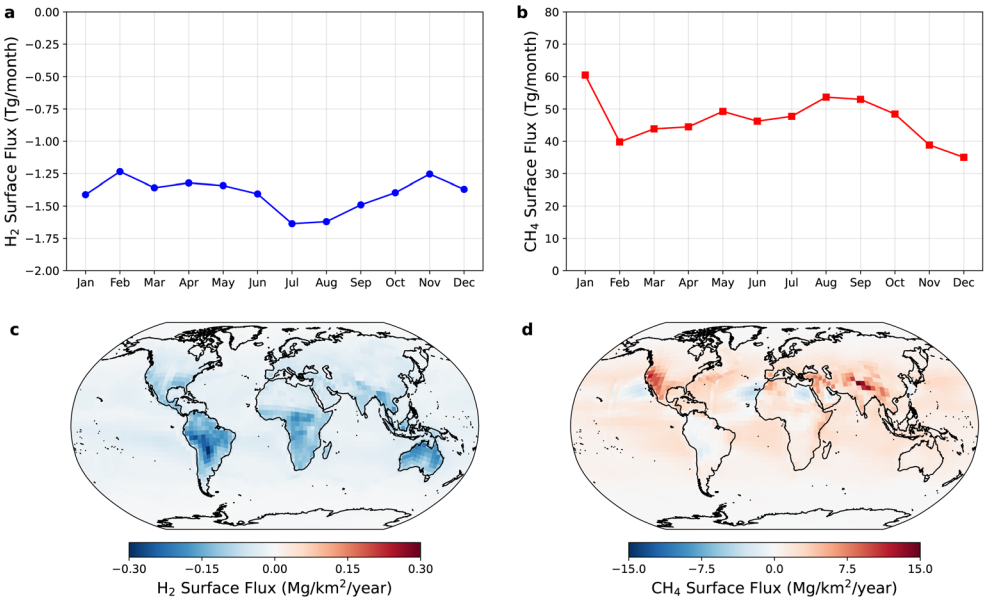

Fig. 1 The calibrated surface fluxes for hydrogen (left, panels (a) and (c)) and methane (right, panels (b) and (d)) required to achieve the prescribed surface mixing ratios for each species. The top panels show the monthly global mean surface fluxes for a sampled simulation year and the bottom panels show the annual mean horizontal distribution of the surface fluxes over the same period.

emission rate, E, of 32.3 Tg H_2 per year, from Paulot *et al.*'s analysis.[8] Based on our average calibrated flux value of −16.8 Tg H_2 per year (Fig. 1), this implies an average soil sink strength of 49.1 Tg H_2 per year, prior to any dynamic uptake scaling. The surface loss term, L, is then calculated as the difference between the emissions and the pre-scaled hydrogen flux.

$$F_{\text{new}} = E - \lambda L$$

$$F_{\text{new}} = E - \lambda(E - F_{\text{old}}) \tag{3}$$

We also develop an additional unsaturated sink model using an exponential relation for the rate of surface uptake of hydrogen in response to increased surface concentrations, which is presented in Section 1 of the SI. This idealized model is used to run a set of sensitivity scenarios in which the surface sink drastically offsets the impact of increased surface hydrogen emissions, representing a near completely unsaturated sink. This model is likely physically unrealistic, but is useful for illustrating the altitude effect under extreme sink behavior. Specifically, when the surface sink responds strongly to higher atmospheric hydrogen levels, more hydrogen gets taken up at the surface before it can react with OH, making the differences between surface and altitude emissions easier to see. This model is intentionally idealized, as it permits excessively strong hydrogen uptake beyond what is supported by observations. Its purpose is not to represent a plausible soil uptake process, but rather to serve as a hypothetical upper bound on soil uptake and to explore the sensitivity of the system to extreme sink behavior, contrasting the Michaelis–Menten scenarios.

2.3 Impact calculations

In this study, we use the perturbation method to calculate the difference in the mass of atmospheric species and the resulting radiative forcing when simulated with and without hydrogen emissions under the various emission and sink assumptions. Although this method does not isolate source-specific impacts due to non-linear interactions within the chemical system, it has been demonstrated to accurately capture the overall chemical response to a given perturbation.[36] By calculating the change in mass of a species between simulations with and without annually-recurring hydrogen emissions, we obtain the step response function ($s(t)$) of the system, and by taking the numerical derivative of the step response function we obtain the impulse response function ($h(t)$). From these results, we calculate the perturbation lifetime (τ_{pert}), defined by IPCC for short-lived forcers[37] as the time taken for the abundance of a species to decrease by 63% ($1\text{–}e^{-1}$) after being perturbed above background levels by a pulse (P_0) of emissions:

$$\tau_{\text{pert}} = \frac{\int_0^\infty h(t)\mathrm{d}t}{P_0} = \frac{s_{\text{ss}}}{P_0} \tag{4}$$

To calculate climate impacts, we use the RRTMG radiative transfer model with stratospheric adjustment as implemented in GCHP to evaluate the changes in radiative forcing for each scenario.[38] Following the implementation by Eastham *et al.*,[27] we assume fixed dynamical heating in the stratosphere and evaluate fluxes at the tropopause.[39] Radiative forcing is calculated every three hours over the first two days of each month, and the resulting twenty-four days of data are used to compute an annual average for each simulation year. The absolute global

Open Access Article. Published on 09 March 2026. Downloaded on 4/20/2026 5:36:04 AM. This article is licensed under a Creative Commons Attribution 3.0 Unported Licence.

warming potential (AGWP) of hydrogen is then calculated directly from the radiative forcing:

$$\mathrm{AGWP}_{\mathrm{H_2}}(\tau) = \int_0^{\tau} \mathrm{RF}_{\mathrm{H_2}}(t)\mathrm{d}t \quad (5)$$

Using the fixed dynamical heating approximation used in RRTMG, the species-specific contributions of methane, water vapor, and ozone to the overall climate impact of hydrogen cannot be isolated. Instead, we use published radiative efficiencies as described in Warwick *et al.*[18] and Forster *et al.*[40] to capture these species contributions. Specifically, we apply fixed radiative efficiencies for methane ($A_{\mathrm{CH_4}} = 3.88 \times 10^{-4}$ W m^{-2} ppb^{-1}), stratospheric water vapor ($A_{\mathrm{H_2O}} = 1.0 \times 10^{-4}$ W m^{-2} ppb^{-1}), and tropospheric ozone ($A_{\mathrm{O_3}} = 0.042$ W m^{-2} DU^{-1}) to compute their respective contributions to the overall climate impact. The radiative efficiencies of each species are integrated with the atmospheric abundances $\Delta[x_i(t)]$ simulated from GCHP to calculate the species-specific AGWP:

$$\mathrm{AGWP}_{\mathrm{H_2},x_i}(\tau) = \int_0^{\tau} A_{x_i}\Delta[x_i(t)]\mathrm{d}t \quad (6)$$

We also calculate the radiative forcing resulting from 1 Tg of annually-recurring CO_2 emissions using the MAGICC6 model.[41] This allows us to compare the integrated climate impacts of the hydrogen emissions to an equivalent mass of CO_2 emissions across different time horizons (τ) using a global warming potential (GWP). We calculate the GWP for hydrogen directly from the integrated radiative forcing of hydrogen and CO_2:

$$\mathrm{GWP}_{\mathrm{H_2}}(\tau) = \frac{\mathrm{AGWP}_{\mathrm{H_2}}(\tau)}{\mathrm{AGWP}_{\mathrm{CO_2}}(\tau)} = \frac{\int_0^{\tau} \mathrm{RF}_{\mathrm{H_2}}(t)\mathrm{d}t}{\int_0^{\tau} \mathrm{RF}_{\mathrm{CO_2}}(t)\mathrm{d}t} \quad (7)$$

For time horizons beyond the 36-year simulation period, we apply an exponential fit to the hydrogen radiative forcing curves to capture steady-state behavior as shown in Fig. 3. Similarly, when using the radiative efficiency method to calculate GWP, we apply an exponential fit to the methane perturbation curve for the saturated sink scenarios. Although most of the response occurs within the simulation period, this extrapolation is needed to capture the final 15% of impacts under the saturated sink scenario. This aligns with findings from literature which show that the methane response to hydrogen (which is the longest-lived mode of impact) decays with an e-folding lifetime of approximately 20 years and falls below 15% of its peak abundance after 35 years.[13,20]

3 Results and discussion

3.1 Impact of soil uptake on atmospheric composition

The global changes to the burdens of hydrogen, methane, stratospheric water vapor, and tropospheric ozone throughout the 36-year simulations are shown in Fig. 2 for each of the scenarios. These changes reflect the integrated response of the atmosphere to 1 Tg of annual-recurring hydrogen emissions under the contrasting soil uptake assumptions described above. We calculate that the total atmospheric hydrogen burden increases between 2.1 Tg and 7.3 Tg across all scenarios at the end of the simulation period, corresponding to increases of 1.3% and 4.4% above present-day levels, respectively. This difference between scenarios is driven by the sink behavior. For the saturated cases, the loss of hydrogen to soil uptake is fixed and non-responsive to rising concentrations, allowing more hydrogen to accumulate in the atmosphere. Specifically, for hydrogen emitted at the surface, the saturated sink scenario (Sur_Sat) results in an increased total hydrogen burden of 7.2 Tg, 3.4 times larger than the increase for the unsaturated sink scenario (Sur_MM). Correspondingly, the global mean surface mixing ratio of hydrogen increases by 6.5 ppbv under the Sur_MM scenario and by 21 ppbv under the Sur_Sat scenario. This sensitivity to the sink saturation is also observed in other key species. For methane, the burden increases from a difference of 2.8 Tg (Sur_MM) to 9.1 Tg (Sur_Sat); for stratospheric water vapor, from 0.28 Tg to 0.97 Tg; and for tropospheric ozone, from 0.13 Tg to 0.42 Tg. These correspond to increases of 3.2×, 3.4×, and 3.3× of the three species respectively, closely tracking the 3.4-fold increase for hydrogen.

Analysis of the perturbation response also reveals a shift in both the timing and magnitude of mass peaks when comparing the saturated and unsaturated sink scenarios. Specifically, the saturated sink leads to a perturbation that is larger in magnitude, occurs later, and decays more slowly. This trend is most pronounced for methane: when the sink becomes saturated, the peak methane abundance shifts from year 4 to year 8, and its peak magnitude increases from 0.19 Tg (67 pptv) to 0.42 Tg (147 pptv). Comparing this peak methane magnitude to previously reported ranges in literature shows general alignment, although the results vary by study and modeling assumptions. For example, Chen *et al.* calculated peak methane abundances of 120 pptv CH_4 per Tg H_2 using a simplified box model, and 71 pptv CH_4 per Tg H_2 when using a more detailed chemical mechanism within the box model.[20] Similarly, Derwent *et al.* and Field and Derwent reported values of 80 pptv CH_4 per Tg H_2 and 27 pptv CH_4 per Tg H_2, respectively, when using higher fidelity models.[17,42]

The shift in the time of the peak methane abundance from 4 to 8 years is due to changes in the removal pathways for both hydrogen and methane. These pathways can be considered with a simplified representation similar to the analysis by Bertagni *et al.*[13] but neglecting reaction with CO and other OH sinks for explanatory purposes, using the equations:

$$\frac{\mathrm{d}[\mathrm{CH_4}]}{\mathrm{d}t} = S_{\mathrm{CH_4}} - k_1[\mathrm{OH}][\mathrm{CH_4}]$$

$$\frac{\mathrm{d}[\mathrm{H_2}]}{\mathrm{d}t} = S_{\mathrm{H_2}} - k_2[\mathrm{OH}][\mathrm{H_2}] - k_{\mathrm{soil}}[\mathrm{H_2}]$$

$$\frac{\mathrm{d}[\mathrm{OH}]}{\mathrm{d}t} = S_{\mathrm{OH}} - k_1[\mathrm{OH}][\mathrm{CH_4}] - k_2[\mathrm{OH}][\mathrm{H_2}]$$

© 2026 The Author(s). Published by the Royal Society of Chemistry

Open Access Article. Published on 09 March 2026. Downloaded on 4/20/2026 5:36:04 AM.
This article is licensed under a Creative Commons Attribution 3.0 Unported Licence.

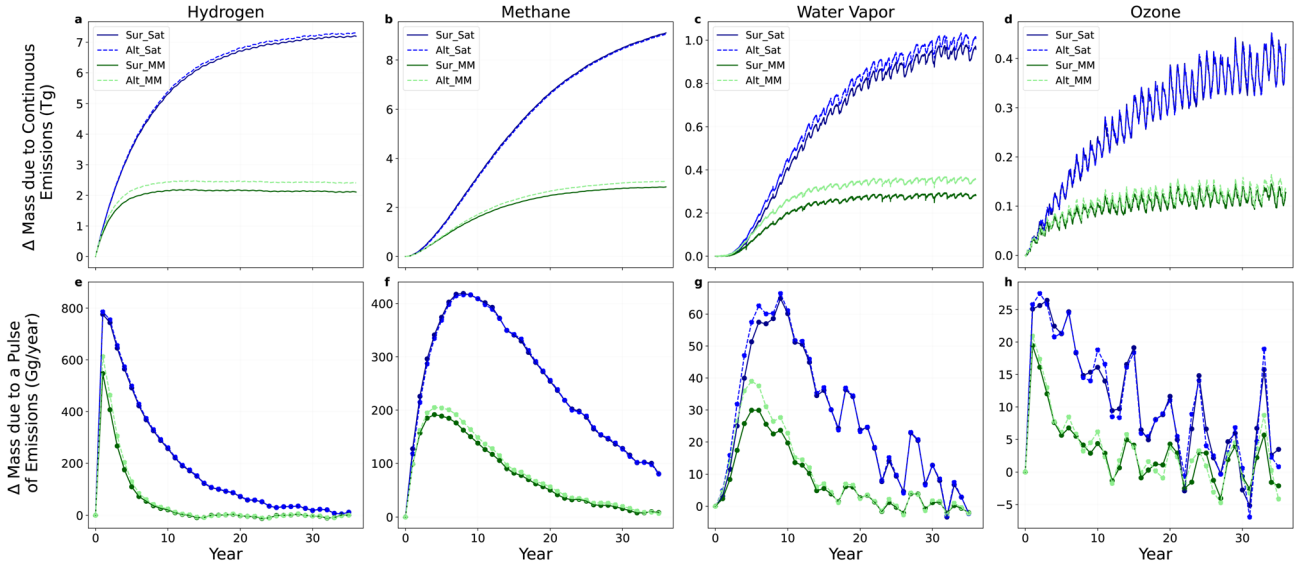

Fig. 2 Changes in the masses of atmospheric hydrogen, methane, stratospheric water vapor, and tropospheric ozone relative to the reference scenario, resulting from 1 Tg of annually recurring hydrogen emissions. The top row (panels (a)–(d)) shows the step response, obtained directly from daily GCHP model output. The bottom row (panels (e)–(h)) shows the corresponding impulse response, calculated as the numerical derivative of the step response averaged over two years. The blue curves and green curves represent the response to the saturated and unsaturated surface sinks, respectively. The light and dark shaded curves represent the response to hydrogen emitted at an altitude of 11 km and at the surface, respectively.

In this simplified case, the sources of hydrogen and methane are fixed and independent of the atmospheric state, as represented by the terms S_{H_2} and S_{CH_4}, respectively. In contrast, the sinks are coupled through the interaction between loss rates to OH (with rate constants k_1 and k_2), the loss rate of hydrogen to soil (k_{soil}), and the atmospheric concentrations of hydrogen, methane, and OH. Under the unsaturated sink, hydrogen is efficiently removed by both chemical oxidation and microbial uptake in soils. However, when the soil sink becomes saturated, this is represented by a proportional reduction in the soil uptake of hydrogen. This manifests in our model as a decrease in the average value of k_{soil} from 0.30 year^{-1} to 0.29 year^{-1}, increasing hydrogen's lifetime against loss to soil from 3.3 years to 3.5 years. Similarly, when comparing hydrogen loss partitioning between soil uptake and OH oxidation, saturation of the soil sink increases the fraction lost to OH from 32.4% to 32.7%. Conversely, the fraction lost to soil decreases from 67.6% to 67.3%. While these changes appear small in absolute terms, they are measured against the total atmospheric hydrogen burden, which is large, meaning that even small changes in the global average can correspond to substantial impacts. We find that this reduction in soil sink strength raises the overall perturbation lifetime of hydrogen (calculated using eqn (4)) from 3.0 years to 8.6 years, increasing its average atmospheric abundance.

The increased atmospheric hydrogen burden is associated with more competition with methane for OH, thus decreasing OH concentrations. This reduction in OH slows down the oxidation of methane, thereby extending its atmospheric lifetime and shifting its peak abundance to a later time. This corresponds to an increase in the methane perturbation lifetime from 12 years to 16 years, though the bulk lifetime of loss against OH is only increased from 6.92 years to 6.93 years. Our methane perturbation lifetime of approximately 12 years for the unsaturated sink scenarios aligns with literature estimates, while the value of 16 years is unsurprisingly higher since previous studies did not focus on sink saturation.[18,19,22,43] Specifically, feedback factors from previous studies on hydrogen's atmospheric impact range between 1.3 and 1.6, and when compared with the modeled bulk lifetime of methane result in perturbation lifetimes ranging from 9.4 years to 12.7 years. Recent studies by Ocko and Hamburg, and Chen *et al.* report methane perturbation lifetimes of 11.8 years and 11.9 years, respectively, closely matching our modeled perturbation lifetime.[10,20]

Conceptually, the mechanism driving the extended perturbation lifetime mirrors the response to direct hydrogen emissions in which emitted hydrogen reduces the availability of OH, prolonging methane's lifetime. However, instead of adding more hydrogen directly through emissions, here we reduce the removal of hydrogen by limiting the soil sink. Both processes result in delayed oxidation of methane. These findings demonstrate the close interaction in which methane and hydrogen are linked not only through their competition for OH, but also through hydrogen's rate of soil uptake. A similar trend is seen in Fig. 2 for stratospheric water vapor and tropospheric ozone, in which an adaptive and stronger soil sink results in impacts that occur sooner, but decay faster. For water vapor, this is demonstrated by the peak abundance being shifted from year 5 to year 9 when the soil sink is saturated, and the perturbation lifetime increasing from 7.5 years to 9.9 years. For ozone, the effect is even greater, with the peak abundance shifting from year 1 to year 3, and the perturbation lifetime increasing from 5.5 years to 13 years.

© 2026 The Author(s). Published by the Royal Society of Chemistry

Open Access Article. Published on 09 March 2026. Downloaded on 4/20/2026 5:36:04 AM.
This article is licensed under a Creative Commons Attribution 3.0 Unported Licence.

3.2 Impact of emission altitude on atmospheric composition

For the unsaturated sink, we calculate that emissions of hydrogen in the upper troposphere (Alt_MM) result in a steady-state hydrogen mass perturbation that is 14% larger than for the equivalent emissions from surface level (Sur_MM). The difference falls to 1.4% when the surface sink is saturated, however. Similarly, when considering the peak perturbation magnitude for methane, stratospheric water vapor, and tropospheric ozone to a pulse of hydrogen emissions, the cruise altitude emissions result in values that are 8.0%, 26%, and 7.9% larger, respectively, than from the equivalent surface emissions. This is driven by increased vertical separation of hydrogen from the soil sink when emitted at altitude. On a per molecule basis, emitting at altitude decreases the likelihood of hydrogen physically encountering the surface, and thus biases the hydrogen towards reaction with OH. This manifests in our model as an increase in the average fractional loss of hydrogen to OH by 0.04%. This change appears small because it is averaged over the full global atmospheric hydrogen burden and reflects only a small emissions perturbation.

The varied response between each species reflects differences in the chemical pathways and transport associated with hydrogen oxidation. Water vapor shows the strongest sensitivity to emission altitude, as hydrogen released at higher altitudes is more likely to reach the stratosphere due to proximity. This effect is most pronounced in the tropics, as shown in Fig. S3. This hydrogen bypasses the tropopause cold trap, which typically limits the upward transport of tropospheric water vapor.[11] Additionally, hydrogen emissions at altitude extend methane's atmospheric lifetime, resulting in increased concentrations of methane in the stratosphere. This increase in stratospheric methane concentration increases the production of stratospheric water vapor due to increased *in situ* methane oxidation, delaying the oxidation of other species in the stratosphere which yield less water vapor from each molecule of OH. This result, however, is sensitive to the assumed sink's degree of responsiveness. If the soil sink becomes saturated, the cruise altitude emissions result in an increased steady-state water vapor perturbation which is 5.5× smaller than the increase in the unsaturated case. For methane and ozone, respectively, the relative increase is 16× and 66× smaller, than for the unsaturated case.

3.3 Impact of background atmosphere on the perturbation response

To evaluate the sensitivity of these perturbations to the background atmosphere, the Sur_MM, Alt_MM, and Sur_Sat scenarios were re-simulated for 9 years using the SSP2-4.5 background atmosphere, representative of the "Middle of the Road" emissions future. This involved a new hydrogen and methane flux calibration simulation, a new reference (no hydrogen perturbation) simulation, as well as the repeated simulation of the three hydrogen emission scenarios. We find that while the magnitude of atmospheric perturbations differs between SSP1-2.6 and SSP2-4.5 background atmospheres, the relative effects of emission altitude and soil sink saturation remain consistent. Specifically, when comparing the step response of these sensitivity simulations after 9 years, the differences between the Sur_MM and Alt_MM scenarios vary by no more than 1.2% between the two background atmospheres. Similarly, when comparing the Sur_MM and Sur_Sat scenarios, the differences remain under 0.7% across the background atmospheres. The step responses of these sensitivity simulations are plotted in Fig. S7.

The magnitude of the atmospheric perturbations, however, does depend on the background atmosphere. Relative to SSP1-2.6 after 9 years, the SSP2-4.5 simulations result in 7–9% smaller hydrogen perturbations, 6% smaller methane perturbations, 4–5% smaller stratospheric water vapor perturbations, and 24–29% smaller tropospheric ozone perturbations for both the Sur_MM and Alt_MM scenarios. The Sur_Sat scenario shows a different pattern, with 5% larger perturbations for hydrogen, water vapor, and methane, but 18% smaller ozone perturbations. With the exception of ozone, these results are comparable in magnitude to the findings by Skeie *et al.*, who examined hydrogen's climate impact across multiple SSP background atmospheres (SSP5-8.5, SSP4-3.4, and SSP1-1.9).[44] Their analysis showed that the resulting variation in hydrogen's GWP-100 remained below 10% across all background scenarios. The increased sensitivity of the ozone response to the background atmosphere in our simulation is unsurprising, given the non-linearity of its production mechanisms with respect to background concentrations. We anticipate a similar sensitivity of our results to other background atmospheres, which may affect the absolute climate impact of future hydrogen emissions but is unlikely to alter the relative effects of emission altitude or soil sink saturation given the uniform offset observed across the scenarios. Future research is recommended to further constrain the magnitude of hydrogen's climate impact given changing background atmospheres, and to explore the parameters that control these effects.

3.4 Climate impacts

The climate impacts resulting from each scenario are calculated using the RRTMG radiative transfer model for the atmospheric response to hydrogen emissions and MAGICC6 for equivalent masses of CO_2 emissions, as described in Section 2.3. These results are shown in Fig. 3, for both the integrated hydrogen climate impacts and the associated global warming potential (GWP) across varying time horizons. By the end of the 100 year period, the radiative forcing resulting from 1 Tg per year of continuous hydrogen emissions reaches a value of 0.84 mW m^{-2}/(Tg $year^{-1}$) for the unsaturated sink (Sur_MM) and 3.17 mW m^{-2}/(Tg $year^{-1}$) for the saturated sink (Sur_Sat). This 3.8-fold difference highlights the sensitivity of hydrogen's climate impact to reduced surface uptake. For the unsaturated sink scenarios, we also show a further 0.11 mW m^{-2}/(Tg $year^{-1}$) increase in the integrated radiative forcing when hydrogen is emitted at altitude compared to as the surface, corresponding to a 13% larger radiative forcing. For the scenarios with a saturated soil sink, this difference is only 1%.

These trends are also reflected in the global warming potentials. We calculate GWP-100 values for hydrogen of 9.2

© 2026 The Author(s). Published by the Royal Society of Chemistry

Open Access Article. Published on 09 March 2026. Downloaded on 4/20/2026 5:36:04 AM.
This article is licensed under a Creative Commons Attribution 3.0 Unported Licence.

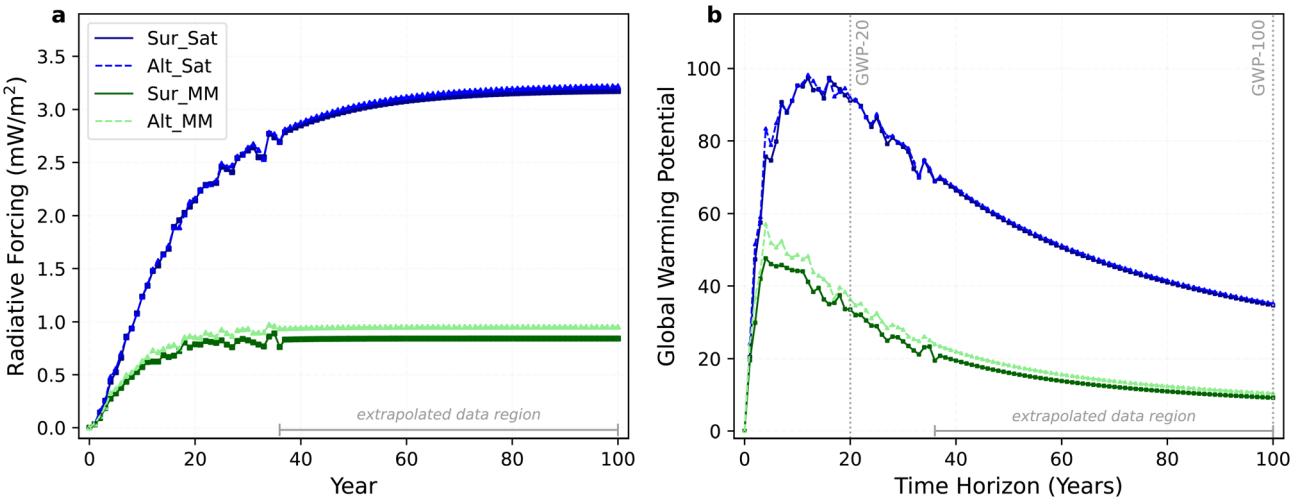

Fig. 3 The stratospherically-adjusted radiative forcing relative to the reference scenario, resulting from 1 Tg of annually recurring hydrogen emissions (a) and the associated GWP of hydrogen over varying time horizons (b). The blue curves and green curves represent the response to the saturated and unsaturated surface sinks, respectively. The light and dark shaded curves represent the response to hydrogen emitted at an altitude of 11 km and at the surface, respectively. An exponential fit is applied to the hydrogen radiative forcing curves beyond year 36.

and 35 for the unsaturated and saturated sinks, respectively, when hydrogen is emitted from the surface. For the unsaturated sink, this GWP-100 is consistent with literature estimates. For example, Sand *et al.*'s multi-model analysis calculated a GWP-100 of 11.6 ± 2.8, with their larger values possibly resulting from variation in representation of soil uptake and its response to atmospheric hydrogen levels compared to our model.[22] In the analysis by Yang *et al.*, GEOS-Chem was used to calculate a GWP-100 for hydrogen of 10.8 using the standard model configuration, or 8.8 when correcting for model OH biases.[23] Since the standard GEOS-Chem configuration of OH reactivity is used in our study, we expect that our quantitative estimates of hydrogen's climate impact may be overestimated within this range. However, because our analysis focuses on differences between perturbation scenarios, systematic OH biases largely cancel and do not affect our primary conclusions regarding relative impacts of sink saturation and emission altitude.[23] Additionally, Yang *et al.* used a fixed surface boundary perturbation approach to resolve sensitivities to hydrogen emissions, making it difficult to directly compare with our method and results. The box modeling performed by Chen *et al.* predicted a GWP-100 of 10^{+7}_{-4}, with the error range reflecting a range of sensitivities in the surface sink strength, temperature, background concentrations and emissions, location, and radiative properties.[20] For the saturated sink scenario, our GWP-100 of 35 is representative if the soil is unable to take up additional hydrogen beyond present-day rates, thus driving the overall climate impact of hydrogen emissions up. This represents a bound for the worst-case scenario for hydrogen's impacts under potential future non-linearities in response to changing environmental conditions.

These results also show a dependence on altitude, where the GWP-100 is increased from 9.2 to 10.4 (a 13% increase) if the emission location is changed from the surface level to 11 km under the unsaturated sink scenario. Similarly to the species changes presented in Section 3.2, the increased climate contribution of hydrogen emitted at high altitude represents a bias towards reaction with OH as opposed to removal by the soil sink due to the physical separation of the loss pathways. If the sink becomes much more responsive to increased atmospheric hydrogen levels, the altitude effect becomes relatively larger as the increased responsiveness of the soil sink further biases surface emissions towards soil uptake. For example, under the scenarios using the exponential surface response model discussed in Section 2 the climate impacts of hydrogen emissions could increase by 240% when emitted at altitude relative to equivalent surface emissions, as shown in Fig. S2. In this case, however, the overall climate impact of hydrogen emissions decreases, with the GWP-100 remaining below 2.5. In contrast, we find that if the surface sink is saturated, the altitude effect disappears and the GWP-100 of hydrogen is the same whether emitted at surface or altitude. Considering a shorter time horizon, we calculate GWP-20 values of 32 and 91 for the unsaturated and saturated sink scenarios respectively, for hydrogen emitted at surface level. For emissions at altitude, the GWP-20 increases by 8% for the unsaturated sink scenario, but is unaffected under the saturated sink scenario. Similar to the 100 year time horizon, the GWP-20 unsaturated sink result of 32 aligns with literature estimates including Chen *et al.*'s projection of 28^{+18}_{-11}, Ocko and Hamburg's calculation of 40^{+20}_{-15} or Warwick *et al.*'s result of 34.4^{+17}_{-15}.[10,18,20] Our GWP-20 calculation of 91 for the saturated sink is 2 to 3 times higher than these literature estimates, again reflecting the increased climate impact associated with an inability for the soil to take up additional hydrogen emissions. The timing of the peak global warming potential also varies between our scenarios, shifting from year 4 to year 16 when the surface sink becomes saturated, reflecting changes in the perturbation lifetime of hydrogen and methane discussed previously.

© 2026 The Author(s). Published by the Royal Society of Chemistry

Open Access Article. Published on 09 March 2026. Downloaded on 4/20/2026 5:36:04 AM.
This article is licensed under a Creative Commons Attribution 3.0 Unported Licence.

We also evaluate the GWP-100 using published radiative efficiencies to isolate the individual contributions of methane, stratospheric water vapor, and tropospheric ozone, as described in Section 2.3. We find that GWP values match the values calculated using RRTMG within 1% for the saturated sink scenarios and 11% for the unsaturated sink scenarios. In all cases, the GWP values are higher when calculated with the radiative efficiencies compared to RRTMG. From the radiative efficiency-based calculations, we show a contribution to the overall GWP-100 of 42–43% from methane, 51–53% from tropospheric ozone, and 6–7% from stratospheric water vapor. These results show a stratospheric water vapor contribution that is lower than the average of 18% presented in the multi-model analysis by Sand *et al.* However, the results are within the expected range of uncertainty.[22] For the unsaturated sink, we find that when hydrogen is emitted at altitude, the absolute global warming potential contribution from stratospheric water vapor increases by 26%, compared to increases of only 8% and 6% for methane and ozone, respectively. This reinforces the behavior discussed previously whereby emissions at altitude result in increased transport of both hydrogen and methane into the stratosphere where they oxidize to produce stratospheric water vapor. Thus, high-altitude hydrogen emissions disproportionately strengthen the stratospheric water vapor pathway by partially bypassing the tropopause cold trap and therefore increasing their climate impact. A graphical breakdown of the GWP-100 and species contribution for the saturated and unsaturated (Michaelis–Menten) simulation calculated using the radiative efficiencies is included in Section 4 of the SI.

4 Conclusion

In this study, we consider the effect of hydrogen uptake by soil microbes, as represented through the surface boundary condition, on the atmospheric response to hydrogen emissions under varying levels of sink responsiveness to increased hydrogen concentrations. We show that if the surface sink becomes saturated (*i.e.*, unable to scale its uptake in response to increasing atmospheric hydrogen concentrations), the overall climate impact of hydrogen increases by a factor of 3.8 due to an extended perturbation lifetime. While complete global saturation is unlikely, this scenario provides an upper bound on the climate impact of hydrogen emissions, and underscores the sensitivity of these impacts to surface removal processes. Moreover, regional reductions in soil uptake due to environmental or land-use changes could lead to localized climate impacts for hydrogen emissions that are several times greater than the global average impact. Accurately capturing this response, however, hinges on understanding how much of the emitted hydrogen is removed *via* chemical oxidation *versus* uptake by the soil sink, which is highly sensitive to the prescribed sink assumptions. Thus, improving future projections of hydrogen's atmospheric impacts requires better constraining of the soil sink and strengthening of confidence in its representation in models, including its response to changing background conditions. Global models that aim to simulate hydrogen emissions and their effects should move beyond fixed surface boundary conditions and instead include an explicit representation of microbial uptake. Without this, models risk misrepresenting both the magnitude and the spatial and temporal variability of hydrogen's removal.

We also demonstrate, for the first time, that emission altitude influences the climate impact of hydrogen emissions due to the vertical separation from the soil sink, biasing hydrogen towards oxidation by OH. In the unsaturated sink scenario, hydrogen emitted at ~11 km results in an 8% greater climate impact over 20 years and a 13% greater impact over 100 years compared to equivalent surface emissions. Similarly, under the unsaturated sink scenario, hydrogen released at cruise altitude leads to a 14% higher steady-state atmospheric hydrogen abundance than equivalent surface emissions. Only when the sink becomes completely saturated does the additional impact of high-altitude emission disappear. These findings suggest that hydrogen emitted from aircraft flying at commercial cruise altitudes warrant greater mitigation attention than equivalent ground-level emissions. In contrast, under the assumption of a fully saturated sink, altitude has no effect, and emissions from aircraft and ground infrastructure can be treated as equivalent. While complete saturation is unlikely, the degree of altitude sensitivity depends on the true response of the soil sink. Given that this is poorly constrained, our results show the need for additional study in this area to inform the aviation sector and broader hydrogen economy.

The sensitivity of these outcomes to the prescribed behavior of the soil sink highlights the need for improved understanding of the true response of the surface sink to varying environmental parameters and background atmospheric composition, as well as how this response may change in the future. To more accurately capture hydrogen's removal processes and downstream effects on methane, ozone, and water vapor, models must move beyond fixed boundary conditions and instead adopt explicit, flux or deposition-based representations of surface uptake. Doing so will be critical for robust assessment of hydrogen's role in future climate scenarios and accurate evaluation of the climate impact of hydrogen-powered aviation.

Author contributions

SDE, FA, RLS, and EMG contributed to conceptualization and acquiring funding. EMG and SDE developed and tested the software and models used in the study. SDE, RLS, and EMG proposed the method and framework. EMG performed the numerical simulations, analyzed and visualized the results, and wrote the original draft. All authors contributed to editing and review of the manuscript.

Conflicts of interest

There are no conflicts to declare.

Data availability

This work was completed using version 14.2.3 of the GEOS-Chem High-Performance (GCHP) code. The specific code base

© 2026 The Author(s). Published by the Royal Society of Chemistry

Open Access Article. Published on 09 March 2026. Downloaded on 4/20/2026 5:36:04 AM. This article is licensed under a Creative Commons Attribution 3.0 Unported Licence.

used can be found at https://doi.org/10.5281/zenodo.17065284. Input data for the GEOS-Chem High Performance model are publicly accessible from https://geoschemdata.wustl.edu/, as described in the GEOS-Chem model documentation (https://gchp.readthedocs.io/en/stable/).

Supplementary information (SI) is available. See DOI: https://doi.org/10.1039/d5ea00139k.

Acknowledgements

The MERRA-2 data used in this study is provided by the Global Modeling and Assimilation Office (GMAO) at NASA Goddard Space Flight Center. The GCHP simulations were performed using the "Svante" cluster, a facility located at MIT's Massachusetts Green High Performance Computing Center and supported by the Center for Sustainability Science and Strategy (https://cs3.mit.edu). The authors would like to acknowledge funding received from Airbus in support of this project.

References

1 K. Calvin, D. Dasgupta, G. Krinner, A. Mukherji, P. W. Thorne, C. Trisos, J. Romero, P. Aldunce, K. Barrett, G. Blanco, W. W. Cheung, S. Connors, F. Denton, A. Diongue-Niang, D. Dodman, M. Garschagen, O. Geden, B. Hayward, C. Jones, F. Jotzo, T. Krug, R. Lasco, Y.-Y. Lee, V. Masson-Delmotte, M. Meinshausen, K. Mintenbeck, A. Mokssit, F. E. Otto, M. Pathak, A. Pirani, E. Poloczanska, H.-O. Pörtner, A. Revi, D. C. Roberts, J. Roy, A. C. Ruane, J. Skea, P. R. Shukla, R. Slade, A. Slangen, Y. Sokona, A. A. Sörensson, M. Tignor, D. Van Vuuren, Y.-M. Wei, H. Winkler, P. Zhai, Z. Zommers, J.-C. Hourcade, F. X. Johnson, S. Pachauri, N. P. Simpson, C. Singh, A. Thomas, E. Totin, P. Arias, M. Bustamante, I. Elgizouli, G. Flato, M. Howden, C. Méndez-Vallejo, J. J. Pereira, R. Pichs-Madruga, S. K. Rose, Y. Saheb, R. Sánchez Rodríguez, D. Ürge Vorsatz, C. Xiao, N. Yassaa, A. Alegría, K. Armour, B. Bednar-Friedl, K. Blok, G. Cissé, F. Dentener, S. Eriksen, E. Fischer, G. Garner, C. Guivarch, M. Haasnoot, G. Hansen, M. Hauser, E. Hawkins, T. Hermans, R. Kopp, N. Leprince-Ringuet, J. Lewis, D. Ley, C. Ludden, L. Niamir, Z. Nicholls, S. Some, S. Szopa, B. Trewin, K.-I. Van Der Wijst, G. Winter, M. Witting, A. Birt, M. Ha, J. Romero, J. Kim, E. F. Haites, Y. Jung, R. Stavins, A. Birt, M. Ha, D. J. A. Orendain, L. Ignon, S. Park, Y. Park, A. Reisinger, D. Cammaramo, A. Fischlin, J. S. Fuglestvedt, G. Hansen, C. Ludden, V. Masson-Delmotte, J. R. Matthews, K. Mintenbeck, A. Pirani, E. Poloczanska, N. Leprince-Ringuet and C. Péan, IPCC, 2023: Climate Change 2023: Synthesis Report, *Contribution of Working Groups I, II and III to the Sixth Assessment Report of the Intergovernmental Panel on Climate Change*, ed. H. Lee and J. Romero, Intergovernmental panel on climate change (ipcc) technical report, Geneva, Switzerland, 2023.

2 T. K. Tromp, R.-L. Shia, M. Allen, J. M. Eiler and Y. L. Yung, *Science*, 2003, **300**, 1740–1742.

3 M. J. Prather, *Science*, 2003, **302**, 581–582.

4 M. G. Schultz, T. Diehl, G. P. Brasseur and W. Zittel, *Science*, 2003, **302**, 624–627.

5 R. Derwent, P. Simmonds, S. O'Doherty, A. Manning, W. Collins and D. Stevenson, *Int. J. Nucl. Hydrogen Prod. Appl.*, 2006, **1**, 57.

6 T. Rahn, J. M. Eiler, K. A. Boering, P. O. Wennberg, M. C. McCarthy, S. Tyler, S. Schauffler, S. Donnelly and E. Atlas, *Nature*, 2003, **424**, 918–921.

7 D. H. Ehhalt and F. Rohrer, *Tellus B*, 2009, **61**, 500.

8 F. Paulot, D. Paynter, V. Naik, S. Malyshev, R. Menzel and L. W. Horowitz, *Int. J. Hydrogen Energy*, 2021, **46**, 13446–13460.

9 F. Paulot, G. Pétron, A. M. Crotwell and M. B. Bertagni, *Atmos. Chem. Phys.*, 2024, **24**, 4217–4229.

10 I. B. Ocko and S. P. Hamburg, *Atmos. Chem. Phys.*, 2022, **22**, 9349–9368.

11 J. Seinfeld and S. Pandis, *Atmospheric Chemistry and Physics : from Air Pollution to Climate Change*, John Wiley & Sons, Inc, New Jersey, 3rd edn, 2016.

12 N. Warwick, P. Griffiths, J. Keeble, A. Archibald, J. Pyle, and K. Shine, 2022, https://www.gov.uk/government/publications/atmospheric-implications-of-increased-hydrogen-use.

13 M. B. Bertagni, S. W. Pacala, F. Paulot and A. Porporato, *Nat. Commun.*, 2022, **13**, 7706.

14 S. Piché-Choquette, J. Tremblay, S. G. Tringe and P. Constant, *PeerJ*, 2016, **4**, e1782.

15 M. B. Bertagni, F. Paulot and A. Porporato, *Global Biogeochem. Cycles*, 2021, **35**, e2021GB006987.

16 C. Greening, M. Berney, K. Hards, G. M. Cook and R. Conrad, *Proc. Natl. Acad. Sci. U. S. A.*, 2014, **111**, 4257–4261.

17 R. G. Derwent, D. S. Stevenson, S. R. Utembe, M. E. Jenkin, A. H. Khan and D. E. Shallcross, *Int. J. Hydrogen Energy*, 2020, **45**, 9211–9221.

18 N. J. Warwick, A. T. Archibald, P. T. Griffiths, J. Keeble, F. M. O'Connor, J. A. Pyle and K. P. Shine, *Atmos. Chem. Phys.*, 2023, **23**, 13451–13467.

19 D. Hauglustaine, F. Paulot, W. Collins, R. Derwent, M. Sand and O. Boucher, *Commun. Earth Environ.*, 2022, **3**, 295.

20 C. Chen, S. Solomon and K. Stone, *Front. Energy Res.*, 2024, **12**, 1463450.

21 R. G. Derwent, *Int. J. Hydrogen Energy*, 2023, **48**, 8328–8341.

22 M. Sand, R. B. Skeie, M. Sandstad, S. Krishnan, G. Myhre, H. Bryant, R. Derwent, D. Hauglustaine, F. Paulot, M. Prather and D. Stevenson, *Commun. Earth Environ.*, 2023, **4**, 203.

23 L. H. Yang, D. J. Jacob, H. Lin, R. Dang, K. H. Bates, J. D. East, K. R. Travis, D. C. Pendergrass and L. T. Murray, *Geophys. Res. Lett.*, 2025, **52**, e2024GL112445.

24 D. S. Lee, G. Pitari, V. Grewe, K. Gierens, J. E. Penner, A. Petzold, M. J. Prather, U. Schumann, A. Bais, T. Berntsen, D. Iachetti, L. L. Lim and R. Sausen, *Atmos. Environ.*, 2010, **44**, 4678–4734.

25 A. Khodayari, S. C. Olsen, D. J. Wuebbles and D. B. Phoenix, *Atmos. Environ.*, 2015, **113**, 135–139.

26 M. J. Prather and J. Hsu, *Science*, 2010, **330**, 952–954.

27 S. D. Eastham, T. Fritz, I. Sanz-Morère, P. Prashanth, F. Allroggen, R. G. Prinn, R. L. Speth and S. R. H. Barrett, *Environ. Sci.: Atmos.*, 2022, **2**, 388–403.

© 2026 The Author(s). Published by the Royal Society of Chemistry

Open Access Article. Published on 09 March 2026. Downloaded on 4/20/2026 5:36:04 AM. This article is licensed under a Creative Commons Attribution 3.0 Unported Licence.

28 M. A. J. Brown, N. J. Warwick and A. T. Archibald, *Geophys. Res. Lett.*, 2025, **52**, e2024GL113653.
29 N. W. Simone, M. E. J. Stettler and S. R. H. Barrett, *Transp. Res. D Trans. Environ.*, 2013, **25**, 33–41.
30 S. D. Eastham, M. S. Long, C. A. Keller, E. Lundgren, R. M. Yantosca, J. Zhuang, C. Li, C. J. Lee, M. Yannetti, B. M. Auer, T. L. Clune, J. Kouatchou, W. M. Putman, M. A. Thompson, A. L. Trayanov, A. M. Molod, R. V. Martin and D. J. Jacob, *Geosci. Model Dev.*, 2018, **11**, 2941–2953.
31 R. Gelaro, W. McCarty, M. J. Suárez, R. Todling, A. Molod, L. Takacs, C. A. Randles, A. Darmenov, M. G. Bosilovich, R. Reichle, K. Wargan, L. Coy, R. Cullather, C. Draper, S. Akella, V. Buchard, A. Conaty, A. M. D. Silva, W. Gu, G.-K. Kim, R. Koster, R. Lucchesi, D. Merkova, J. E. Nielsen, G. Partyka, S. Pawson, W. Putman, M. Rienecker, S. D. Schubert, M. Sienkiewicz and B. Zhao, *J. Clim.*, 2017, **30**, 5419–5454.
32 V. Eyring, S. Bony, G. A. Meehl, C. A. Senior, B. Stevens, R. J. Stouffer and K. E. Taylor, *Geosci. Model Dev.*, 2016, **9**, 1937–1958.
33 Z. Ouyang, R. B. Jackson, M. Saunois, J. G. Canadell, Y. Zhao, C. Morfopoulos, P. B. Krummel, P. K. Patra, G. P. Peters, F. Dennison, T. Gasser, A. T. Archibald, V. Arora, G. Baudoin, N. Chandra, P. Ciais, S. J. Davis, S. Feron, F. Guo, D. Hauglustaine, C. D. Jones, M. W. Jones, E. Kato, D. Kennedy, J. Knauer, S. Lienert, D. Lombardozzi, J. R. Melton, J. E. M. S. Nabel, M. O'Sullivan, G. Pétron, B. Poulter, J. Rogelj, D. Sandoval Calle, P. Smith, P. Suntharalingam, H. Tian, C. Wang and A. Wiltshire, *Nature*, 2025, **648**, 616–624.
34 M. Saunois, A. R. Stavert, B. Poulter, P. Bousquet, J. G. Canadell, R. B. Jackson, P. A. Raymond, E. J. Dlugokencky, S. Houweling, P. K. Patra, P. Ciais, V. K. Arora, D. Bastviken, P. Bergamaschi, D. R. Blake, G. Brailsford, L. Bruhwiler, K. M. Carlson, M. Carrol, S. Castaldi, N. Chandra, C. Crevoisier, P. M. Crill, K. Covey, C. L. Curry, G. Etiope, C. Frankenberg, N. Gedney, M. I. Hegglin, L. Höglund-Isaksson, G. Hugelius, M. Ishizawa, A. Ito, G. Janssens-Maenhout, K. M. Jensen, F. Joos, T. Kleinen, P. B. Krummel, R. L. Langenfelds, G. G. Laruelle, L. Liu, T. Machida, S. Maksyutov, K. C. McDonald, J. McNorton, P. A. Miller, J. R. Melton, I. Morino, J. Müller, F. Murguia-Flores, V. Naik, Y. Niwa, S. Noce, S. O'Doherty, R. J. Parker, C. Peng, S. Peng, G. P. Peters, C. Prigent, R. Prinn, M. Ramonet, P. Regnier, W. J. Riley, J. A. Rosentreter, A. Segers, I. J. Simpson, H. Shi, S. J. Smith, L. P. Steele, B. F. Thornton, H. Tian, Y. Tohjima, F. N. Tubiello, A. Tsuruta, N. Viovy, A. Voulgarakis, T. S. Weber, M. van Weele, G. R. van der Werf, R. F. Weiss, D. Worthy, D. Wunch, Y. Yin, Y. Yoshida, W. Zhang, Z. Zhang, Y. Zhao, B. Zheng, Q. Zhu, Q. Zhu and Q. Zhuang, *Earth Syst. Sci. Data*, 2020, **12**, 1561–1623.
35 K. A. Johnson and R. S. Goody, *Biochemistry*, 2011, **50**, 8264–8269.
36 V. Grewe, K. Dahlmann, S. Matthes and W. Steinbrecht, *Atmos. Environ.*, 2012, **59**, 102–107.
37 S. Szopa, V. Naik, B. Adhikary, P. Artaxo, T. Berntsen, W. Collins, S. Fuzzi, L. Gallardo, A. Kiendler-Scharr, Z. Klimont, H. Liao, N. Unger and P. Zanis, *Climate Change 2021 – The Physical Science Basis: Working Group I Contribution to the Sixth Assessment Report of the Intergovernmental Panel on Climate Change*, Cambridge university press technical report, 2023.
38 C. L. Heald, D. A. Ridley, J. H. Kroll, S. R. H. Barrett, K. E. Cady-Pereira, M. J. Alvarado and C. D. Holmes, *Atmos. Chem. Phys.*, 2014, **14**, 5513–5527.
39 S. B. Fels, J. D. Mahlman, M. D. Schwarzkopf and R. W. Sinclair, *J. Atmos. Sci.*, 1980, **37**(10), 2265–2297.
40 P. Forster, T. Storelvmo, K. Armour, W. Collins, J.-L. Dufresne, D. Frame, D. Lunt, M. Thorsten, M. Palmer, M. Watanabe, M. Wild and H. Zhang, *Climate Change 2021 – The Physical Science Basis: Working Group I Contribution to the Sixth Assessment Report of the Intergovernmental Panel on Climate Change*, Cambridge university press technical report, 2021.
41 M. Meinshausen, S. C. B. Raper and T. M. L. Wigley, *Atmos. Chem. Phys.*, 2011, **11**, 1417–1456.
42 R. Field and R. Derwent, *Int. J. Hydrogen Energy*, 2021, **46**, 30190–30203.
43 R. G. Derwent, W. J. Collins, C. E. Johnson and D. S. Stevenson, *Clim. Change*, 2001, **49**, 463–487.
44 R. B. Skeie, M. Sandstad, S. Krishnan, G. Myhre and M. Sand, *Atmos. Chem. Phys.*, 2025, **25**, 4929–4942.

 © 2026 The Author(s). Published by the Royal Society of Chemistry